Mathematics and Computers in Simulation 221 (2024) 589–605

Contents lists available at ScienceDirect

Mathematics and Computers in Simulation

journal homepage: www.elsevier.com/locate/matcom

Original articles

Comoving mesh method for multi-dimensional moving boundary problems: Mean-curvature flow and Stefan problems

Yosuke Sunayama [a], Julius Fergy Tiongson Rabago [b,*], Masato Kimura [b]

[a] PFU Limited, Nu 98-2 Unoke, Kahoku, 929-1192, Ishikawa, Japan
[b] Faculty of Mathematics and Physics, Institute of Science and Engineering, Kanazawa University, Kakumamachi, Kanazawa, 920-1192, Ishikawa, Japan

ARTICLE INFO

Keywords:
Comoving mesh method
Moving boundary problem
Mean-curvature flow
Stefan problem

ABSTRACT

The "comoving mesh method" or CMM is a Lagrangian-type numerical scheme recently developed for numerically solving classes of moving boundary problems. The scheme is well-suited for solving, for example, the Hele-Shaw flow problem, the curve-shortening problem, and the well-known Bernoulli free boundary problem. This finite element method exploits the idea that the normal velocity field of a moving boundary can be extended smoothly throughout the entire domain of the problem's definition using, for instance, the Laplace operator. By doing so, the finite element mesh of the domain is easily updated at every time step by moving the nodal points along this velocity field. As a result, one avoids the need to generate a new computational mesh at every time step. In this exposition, we further develop and demonstrate the practicality of the method by solving moving boundary problems set in higher dimensions and its application to solving the Stefan problem in two dimensions. Numerical examples are provided for illustration purposes.

1. Introduction

The main objective of this work is to reintroduce the comoving mesh method (CMM) [27] and showcase its application to time-dependent moving boundary problems (MBPs). While a previous study [27] focused on two-dimensional and time-independent problems, our aim is to demonstrate the method's versatility in higher dimensions and for time-dependent cases. Specifically, we are interested in examining the mean-curvature flow problem (MCF) and the well-known one-phase Stefan problem.

1.1. Background and model problems

Let $T > 0$ be fixed and B be an open bounded set (which can be empty) in $\mathbb{R}^d$ $(d = 2, 3)$ with a smooth boundary ∂B. For $t \in I_T := [0, T]$, consider a larger open bounded set $\Omega(t) \subset \mathbb{R}^d$ containing $\overline{B}$ with smooth boundary $\Gamma(t) := \partial\Omega(t)$ such that $\mathrm{dist}(\partial B, \Gamma(0)) > 0$.

Given the functions $f : \mathbb{R}^d \times I_T \to \mathbb{R}$, $q_B : \partial B \times I_T \to \mathbb{R}$, $g : \mathbb{R} \times I_T \to \mathbb{R}$, $\boldsymbol{\gamma} : \mathbb{R}^d \times I_T \to \mathbb{R}^d$, the constant $\lambda \in \mathbb{R}$, and the initial profile $\Omega^0 := \Omega(0)$ of $\Omega(t)$, with $V_n := V_n(x, t)$, $x \in \Gamma(t)$, describing the outward normal velocity of the moving interface $\Gamma(t)$, we consider the following MBP:

* Corresponding author.
E-mail addresses: jftrabago@gmail.com, rabagojft@se.kanazawa-u.ac.jp (J.F.T. Rabago).

https://doi.org/10.1016/j.matcom.2024.03.020
Received 15 August 2023; Received in revised form 20 February 2024; Accepted 13 March 2024
Available online 16 March 2024

Problem 1.1.1. Find $\Omega(t) \supset \overline{B}$ and $u(\cdot,\ t) : \overline{\Omega(t)} \setminus B \to \mathbb{R}$ such that

$$\begin{cases} -\Delta u = f & \text{in } \Omega(t) \setminus \overline{B}, \quad t \in I_T, \\ (1-\alpha)u + \alpha \nabla u \cdot \nu = q_B & \text{on } \partial B, \\ u = g & \text{on } \Gamma(t), \quad t \in I_T, \\ V_n = (-\nabla u + \boldsymbol{\gamma}) \cdot \nu + \lambda & \text{on } \Gamma(t), \quad t \in I_T, \\ \Omega(0) = \Omega^0, \end{cases} \tag{1}$$

where $\alpha \in \{0, 1\}$ which indicates a Dirichlet ($\alpha = 0$) or a Neumann boundary condition ($\alpha = 1$) is used, and ν denotes the outward unit normal vector on the boundary of $\Omega(t) \setminus \overline{B}$.

A particular case of Problem 1.1.1 is the well-known Hele-Shaw problem (see, e.g., [10]) which is recovered by taking $f \equiv 0$, $g \equiv 0$, $\boldsymbol{\gamma} \equiv \mathbf{0}$ and $\lambda = 0$ in Eq. (1). Meanwhile, if one takes $f = f(x)$, $g \equiv 0$, $\boldsymbol{\gamma} \equiv \mathbf{0}$, and $\lambda < 0$ in (1), then the system of equation is related to the exterior case of the Bernoulli problem [11,12,20] (a.k.a. the Alt-Caffarelli problem). In fact, if one supposes that the solution to (1) converges to a stationary point Ω^* (i.e., Ω^* is a domain such that $V_n = 0$ on $\Gamma^* = \partial\Omega^*$) as t goes to infinity, then Problem 1.1.1 rewrites into the following free boundary problem.

Problem 1.1.2. Given a constant $\lambda < 0$ and a fixed open bounded set B, find a bounded domain $\Omega \supset \overline{B}$ and a function $u : \overline{\Omega} \setminus B \to \mathbb{R}$ such that

$$\begin{cases} -\Delta u = f & \text{in } \Omega \setminus \overline{B}, \\ (1-\alpha)u + \alpha \nabla u \cdot \nu = q_B & \text{on } \partial B, \\ u = 0 \quad \text{and} \quad \nabla u \cdot \nu = \lambda & \text{on } \Gamma. \end{cases} \tag{2}$$

Numerical methods for solving specific cases of Problem 1.1.1 have been extensively studied. The Hele-Shaw problem, for example, has been addressed using the boundary element method (BEM) [15,17,19], the charge simulation method (CSM) or method of fundamental solutions [24–26]. The method from [17] is applicable to other two-dimensional MBPs but becomes computationally demanding in three dimensions. Generalizing these methods to more complex problems, especially in three dimensions, is challenging. Another method suitable for cases where the free boundary can be represented by a graph or a height function was proposed in [5]. This *adaptive* mesh method efficiently applies to two-dimensional scenarios.

Drawing inspiration from the aforementioned studies, we aim to demonstrate in this study the practicality and flexible nature of CMM when applied to diverse moving boundary problems. In doing so, we will illustrate the following attributes of this approach:

- firstly, the method easily applies to higher dimensional MBPs, and does not involve cumbersome ad hoc procedures;
- secondly, the scheme does not require mesh regeneration;
- and, lastly, it can easily be adapted to solve time-dependent MBPs.

Methods for numerically solving MBPs can be categorized into two groups: (i) moving-grid methods, and (ii) fixed-grid methods. [27] provides a brief overview of where CMM stands in the literature. As described in [27], CMM is a type of moving-grid approach. It involves moving nodal points within a discretized domain according to the boundary motion in the normal direction. This method aligns with the concept of the Lagrangian method used in fluid flow problems and relies on smooth extensions. CMM is closely related to the *elliptic-grid generation* (EGG) method, as outlined in [21, Chapter 6], and the *traction method* developed by Azegami [1] for shape optimization problems (see also [2]).

The rest of the paper is organized as follows. In the next Section 1.2, we review some properties obtained in a previous study [27]. Subsequently, in Section 1.3, we recall the motivation and the main idea behind CMM. Moving on to Section 2, we present the application of CMM to solving MCF problems, including its corresponding numerical algorithm. We illustrate the feasibility of the method through numerical examples. In Section 3, we discuss how CMM can solve the one-phase Stefan problem and examine the order of the error of its convergence using numerical examples. Additionally, in Section 4, we investigate a smooth extension of normal flows obtained via the linear elasticity equation, revealing more properties of CMM. Lastly, we conclude the paper in Section 5 and provide a statement of future work.

1.2. Properties of CMM

Prior to unveiling the new features of CMM that we aim to present in this study, we will initially provide a concise overview of its qualitative characteristics that were previously established in [27]. The initial concern pertains to the convergence towards a stationary point Γ^* of the moving boundary $\Gamma(t)$, $t \geqslant 0$. This is discussed within a broader context that involves a general representation of the normal flow V_n. On the other hand, the second concern, known as the ε-approximation property of CMM [27], relates to the scheme's characteristics concerning the well-known Bernoulli problem [8]. This property is applicable to CMM and can be found in Section 3.1 of [27].

Hereafter, we consider the following abstract autonomous moving boundary problem.

Problem 1.2.1. Given an initial surface Γ^0 and a real-valued function $F(\cdot\,; \Gamma) : \Gamma \to \mathbb{R}$, find a moving surface $\Gamma(t)$ with the normal speed V_n, $t \geqslant 0$, which satisfies

$$\begin{cases} V_n(x,t) = F(x; \Gamma(t)), \quad x \in \Gamma(t), \quad t \geqslant 0, \\ \Gamma(0) = \Gamma^0. \end{cases} \tag{3}$$

Specific forms of $F(x;\Gamma(t))$ that are of interest are as follows:

- $F(x;\Gamma(t)) = (-\nabla u + \boldsymbol{\gamma})\cdot\nu + \lambda$ in (1);
- $F(x;\Gamma(t)) = -\kappa$ in (16).

Let us now define what we mean by a stationary solution to Problem 1.2.1.

Definition 1.2.1. A domain Ω^* is said to be a *stationary solution* to Problem 1.2.1 if $\Gamma^* = \partial\Omega^*$, and $F(x;\Gamma^*) = 0$ for almost every $x \in \Gamma^*$.

We associate with Problem 1.2.1 the ε-regularized moving boundary problem given as follows:

Problem 1.2.2. Let B and Ω be two bounded domains with respective Lipschitz boundary ∂B and $\Gamma := \partial\Omega$ such that $\overline{B} \subset \Omega$. Given Γ^0, a real-valued function $F(\cdot;\Gamma) \in L^2(\Gamma)$, and a fix number $\varepsilon > 0$, we seek to find a moving surface $\Gamma(t)$, which satisfies

$$\begin{cases} -\Delta \mathbf{w} = \mathbf{0} & \text{in } \Omega(t)\setminus\overline{B}, \quad t \geqslant 0,\\ \mathbf{w} = \mathbf{0} & \text{on } \partial B,\\ \varepsilon\nabla\mathbf{w}\cdot\nu + \mathbf{w} = F(\cdot;\Gamma(t))\nu & \text{on } \Gamma(t), \quad t \geqslant 0,\\ V_n = \mathbf{w}\cdot\nu & \text{on } \Gamma(t), \quad t \geqslant 0. \end{cases} \tag{4}$$

The positive number ε is referred to here as the CMM parameter. With respect to Problem 1.2.2, a stationary solution Ω^* is define as follows.

Definition 1.2.2. A domain Ω^* is said to be a *stationary solution* to Problem 1.2.2 if $\Gamma^* = \partial\Omega^*$, and $\mathbf{w} \in H^1_{\partial B,\mathbf{0}}(\Omega^*\setminus\overline{B};\mathbb{R}^d)$ solves the variational equation

$$\varepsilon\int_{\Omega^*\setminus\overline{B}} \nabla\mathbf{w} : \nabla\boldsymbol{\varphi}\, dx + \int_{\Gamma^*} \mathbf{w}\cdot\boldsymbol{\varphi}\, \mathrm{d}s = \int_{\Gamma^*} F(\cdot;\Gamma^*)\nu\cdot\boldsymbol{\varphi}\, \mathrm{d}s, \quad \forall\boldsymbol{\varphi} \in H^1_{\partial B,\mathbf{0}}(\Omega^*\setminus\overline{B};\mathbb{R}^d), \tag{5}$$

$$\text{with} \qquad \mathbf{w}\cdot\nu = 0 \quad \text{on } \Gamma^*. \tag{6}$$

For Lipschitz domain $\Omega^*\setminus\overline{B}$ and $F(\cdot;\Gamma) \in L^2(\Gamma)$, Eq. (5) can be shown to have a weak solution $\mathbf{w} \in H^1(\Omega^*\setminus\overline{B};\mathbb{R}^d)$ via Lax–Milgram lemma. With this definition of a stationary point given, one obtains the following.

Proposition 1.2.1 ([27, Prop. 3]). *We suppose $\Omega^* \supset \overline{B}$, $\Gamma^* = \partial\Omega^*$ is Lipschitz, and $F(\cdot;\Gamma) \in L^2(\Gamma)$. Then, the following conditions are equivalent:*

(i) Ω^* is a stationary solution to Problem 1.2.1,
(ii) Ω^* is stationary solution to Problem 1.2.2, for any $\varepsilon > 0$,
(iii) Ω^* is stationary solution to Problem 1.2.2, for some $\varepsilon > 0$.

For the ε-approximation property of CMM, let us again fix Ω and B and suppose that their respective boundaries Γ and ∂B are Lipschitz regular. Given a function $\mathbf{g} : \Gamma \to \mathbb{R}^d$, the said property of CMM is simply concern about the convergence of the Robin approximation to the original Dirichlet boundary condition associated with the following system of PDEs:

$$-\Delta\mathbf{v} = \mathbf{0} \quad \text{in } \Omega\setminus\overline{B}, \qquad \mathbf{v} = \mathbf{0} \quad \text{on } \partial B, \qquad \mathbf{v} = \mathbf{g} \quad \text{on } \Gamma. \tag{7}$$

The corresponding variational equation of (7) admits a unique weak solution $\mathbf{v} \in H^1(\Omega\setminus\overline{B};\mathbb{R}^d)$ for any given data $\mathbf{g} \in H^{1/2}(\Gamma;\mathbb{R}^d)$ and Lipschitz domain $\Omega\setminus\overline{B}$. This follows immediately from the application of Lax–Milgram lemma.

Let us consider system (7) and denote its solution, depending on $\mathbf{g} \in H^{1/2}(\Gamma;\mathbb{R}^d)$, by $\mathbf{v}^i := \mathbf{v}(\mathbf{g}^i)$ and define the Dirichlet-to-Neumann map $\Lambda : H^{1/2}(\Gamma;\mathbb{R}^d) \to H^{-1/2}(\Gamma;\mathbb{R}^d)$. Then, the following lemma holds true:

Lemma 1.2.1 ([27, Lem. 1]). *For $\mathbf{g}^1, \mathbf{g}^2 \in H^{1/2}(\Gamma;\mathbb{R}^d)$, the map*

$$(\cdot,\cdot)_\Lambda : H^{1/2}(\Gamma;\mathbb{R}^d)\times H^{1/2}(\Gamma;\mathbb{R}^d) \to \mathbb{R}, \qquad (\mathbf{g}^1,\mathbf{g}^2)_\Lambda := (\Lambda\mathbf{g}^1,\mathbf{g}^2)_{L^2(\Gamma;\mathbb{R}^d)},$$

is an inner product on $H^{1/2}(\Gamma;\mathbb{R}^d)$, and is equivalent to the $H^{1/2}(\Gamma;\mathbb{R}^d)$-norm.

Now, for $\varepsilon > 0$ and $\mathbf{g} \in H^{1/2}(\Gamma;\mathbb{R}^d)$, we define $\mathbf{g}_\varepsilon$ such that $\varepsilon\Lambda\mathbf{g}_\varepsilon + \mathbf{g}_\varepsilon = \varepsilon\nabla\mathbf{v}_\varepsilon\cdot\nu + \mathbf{v}_\varepsilon =: \mathbf{g}$, and system (7) with $\mathbf{v}$ and $\mathbf{g}$ replaced by $\mathbf{v}_\varepsilon$ and $\mathbf{g}_\varepsilon$, respectively, and, instead of the Dirichlet condition, we imposed on Γ the Robin condition $\varepsilon\nabla\mathbf{v}_\varepsilon\cdot\nu + \mathbf{v}_\varepsilon = \mathbf{g}$. More precisely, we consider the mixed Dirichlet–Robin problem

$$-\Delta\mathbf{v}_\varepsilon = \mathbf{0} \quad \text{in } \Omega\setminus\overline{B}, \quad \mathbf{v}_\varepsilon = \mathbf{0} \quad \text{on } \partial B, \quad \varepsilon\nabla\mathbf{v}_\varepsilon\cdot\nu + \mathbf{v}_\varepsilon = \mathbf{g} \quad \text{on } \Gamma. \tag{8}$$

Let us define the bilinear form $a^\varepsilon(\cdot,\cdot)$ as follows:

$$a^\varepsilon(\boldsymbol{\varphi},\boldsymbol{\psi}) := {}_{H^{-1/2}}\langle(\varepsilon\Lambda + \mathbf{I})\boldsymbol{\varphi},\boldsymbol{\psi}\rangle_{H^{1/2}} = \varepsilon(\boldsymbol{\varphi},\boldsymbol{\psi})_\Lambda + (\boldsymbol{\varphi},\boldsymbol{\psi})_{L^2(\Gamma;\mathbb{R}^d)}.$$

Then, we may write a weak formulation on Γ for $\mathbf{g}^\epsilon$ as follows: find $\mathbf{g}^\epsilon \in H^{1/2}(\Gamma;\mathbb{R}^d)$ such that

$$a^\epsilon(\mathbf{g}^\epsilon, \boldsymbol{\varphi}) = (\mathbf{g}, \boldsymbol{\varphi})_{L^2(\Gamma;\mathbb{R}^d)}, \qquad \text{for all } \boldsymbol{\varphi} \in H^{1/2}(\Gamma;\mathbb{R}^d). \tag{9}$$

Again, the existence of unique weak solution $\mathbf{g}^\epsilon \in H^{1/2}(\Gamma;\mathbb{R}^d)$ to the above variational problem can be proven using Lax–Milgram lemma.

Using Lemma 1.2.1, one derives without difficulty the following convergence property of CMM:

Proposition 1.2.2 (*[27, Prop. 4]*). *Let $\mathbf{g} \in H^{1/2}(\Gamma;\mathbb{R}^d)$ and Γ be Lipschitz regular. If $\Lambda\mathbf{g} \in L^2(\Gamma;\mathbb{R}^d)$, then $\|\mathbf{g}^\epsilon - \mathbf{g}\|_{L^2(\Gamma;\mathbb{R}^d)} \leqslant \epsilon \|\Lambda\mathbf{g}\|_{L^2(\Gamma;\mathbb{R}^d)}$.*

1.3. Motivation and the main idea behind CMM

In this section, we will provide a summary of the concept and the motivation behind the approach, along with its numerical execution, replicating various aspects discussed in [27].

To explain the method with simplicity, we consider Problem 1.1.1 with $\alpha = 1$, $\lambda = 0$, and $\boldsymbol{\gamma} = \mathbf{0}$. Let $T > 0$ be a given final time of interest, N_T a fixed positive integer, and $\tau = T/N_T$ (note that this can be set differently) denotes the desired time discretization step-size. For each time-step index $k = 0, 1, \dots, N_T$, the time-discretized version of domains, boundaries, and functions will be denoted with superscript k (e.g., $\Omega^k \approx \Omega(k\tau)$ and $u^k \approx u(\cdot, k\tau)$). Moreover, we will occasionally write $X = \Omega \setminus \overline{B}$ and its triangulation (with maximum mesh size $h > 0$) as $X_h = \Omega_h \setminus \overline{B}_h$. Throughout the paper, whenever there is no confusion, the subscript h and superscript k will be dropped for ease of writing.

Now let T, N_T, ϵ, and the known functions be fixed, and Ω^0 be given. A naive numerical method to solve (1) is given as follows:

Conventional scheme for the (1)

For $k = 0, 1, \dots, N_T$, do the following:

Step 1. First, find u^k in $\Omega^k \setminus \overline{B}$ that solves the equation

$$-\Delta u^k = f^k \ \text{ in } \Omega^k \setminus \overline{B}, \quad \nabla u^k \cdot \nu^k = q_B^k \ \text{ on } \partial B, \quad u^k = 0 \ \text{ on } \Gamma^k.$$

Step 2. Then, define the normal velocity $V_n^k := -\nabla u^k \cdot \nu^k$ on Γ^k.

Step 3. Finally, update the moving boundary according to

$$\Gamma^{k+1} := \left\{ x + \tau V_n^k(x)\nu^k(x) \;\middle|\; x \in \Gamma^k \right\}.$$

As pointed out in [27], there are two issues in implementing the above scheme in a finite element method (FEM):

- If $u_h^k \in \mathbb{P}_1(\Gamma_h^k)$, then, at time step k, $V_n^k \in \mathbb{P}_0(\Gamma_h^k)$ where Γ_h^k denotes the triangulation of the exterior boundary of $\Omega_h^k \setminus \overline{B}_h$. In this situation, the FE space $\mathbb{P}_0$ is not enough to uniquely define V_n^k on nodal points of the mesh. In fact, we need it to be in $\mathbb{P}_1(\Gamma_h^k)$ FE space in Step 3 of the scheme.
- Typically, FEM for MBPs requires mesh regeneration. While such procedure is not costly in 2D, it is obviously not the case in 3D.

To handle these issues, the following solutions were offered by the authors in [27]. For the second point, one simply needs to move not only the boundary nodes of the mesh, but also its internal nodes at every time step. To do this, a smooth extension $\mathbf{w}$ (dropping the time index k) of $V_n\nu$ in the entirety of X has to be constructed. In CMM, this is done by finding $\mathbf{w}_h \in \mathbb{P}_1(X_h;\mathbb{R}^d)$ which solves, for example, the Laplace equation

$$-\Delta\mathbf{w}_h = \mathbf{0} \ \text{ in } X_h, \qquad \mathbf{w}_h = \mathbf{0} \ \text{ on } \partial B_h, \qquad \mathbf{w}_h = V_n\nu \ \text{ on } \Gamma_h. \tag{10}$$

Then, for each $k = 0, 1, \dots, N_T$, the mesh triangulation $\mathcal{T}_h(\overline{\Omega}_h^{k+1} \setminus B_h) = \{K_l^{k+1}\}_{l=1}^{N_e}$ (N_e the number of elements) of $\overline{\Omega}_h^{k+1} \setminus B_h$ are defined as follows:

$$\overline{\Omega}_h^{k+1} \setminus B_h := \left\{ x + \tau\mathbf{w}_h^k(x) \;\middle|\; x \in \overline{\Omega}_h^k \setminus B_h \right\}, \tag{11}$$

$$K_l^{k+1} := \left\{ x + \tau\mathbf{w}_h^k(x) \;\middle|\; x \in K_l^k \right\}. \tag{12}$$

Remark 1.3.1. If $\mathbf{w}_h^k$ belongs to higher order FE space, then, instead of (12), we define $\mathcal{T}_h(\overline{\Omega}_h^k \setminus B_h)$ with the set of nodal points $\mathcal{N}_h^k = \{p_j^k\}_{j=1}^{N_p}$:

$$\mathcal{T}_h(\overline{\Omega}_h^{k+1} \setminus B_h) := \begin{cases} p_j^{k+1} := p_j^k + \tau \mathbf{w}_h^k(p_j^k) \\ K_l^{k+1} \cap \mathcal{N}_l^{k+1} = K_l^k \cap \mathcal{N}_l^k. \end{cases} \tag{13}$$

On the other hand, to address the first issue, we have proposed in [27] to apply a Robin approximation of the Dirichlet boundary equation on the moving boundary. On this purpose, we fixed a real number $\varepsilon > 0$ and replace the equation $\mathbf{w} = V_n\nu$ by $\varepsilon\nabla\mathbf{w}\cdot\nu + \mathbf{w} = V_n\nu$ on Γ^k in (10). Doing so leads us to finding $\mathbf{w}_h \in \mathbb{P}_1(X_h;\mathbb{R}^d)$ which solves the following system:

$$\begin{cases} -\Delta\mathbf{w}_h = \mathbf{0} & \text{in } \overline{\Omega}_h \setminus B_h, \\ \mathbf{w}_h = \mathbf{0} & \text{on } \partial B_h, \\ \varepsilon\nabla\mathbf{w}_h \cdot \nu_h + \mathbf{w}_h = V_n\nu & \text{on } \Gamma_h. \end{cases} \tag{14}$$

For convenience, let us define the bilinear form $a_{X,Y}(\boldsymbol{\varphi},\boldsymbol{\psi})$ – which is continuous and coercive on associated space – as follows:

$$a_{X,Y}(\boldsymbol{\varphi},\boldsymbol{\psi}) = \int_X \nabla\mathbf{w} : \nabla\boldsymbol{\varphi}\, dx + \frac{1}{\varepsilon}\int_Y \mathbf{w}\cdot\boldsymbol{\varphi}\, ds.$$

The weak formulation of (14) is stated as follows:

$$\begin{cases} \text{find } \mathbf{w} \in H^1_{\partial B,\mathbf{0}}(X_h;\mathbb{R}^d) \text{ such that} \\ \quad a_{X_h,\Gamma_h}(\mathbf{w},\boldsymbol{\varphi}) = \dfrac{1}{\varepsilon}\displaystyle\int_{\Gamma_h} V_n\nu\cdot\boldsymbol{\varphi}\, ds, \quad \text{for all } \boldsymbol{\varphi} \in H^1_{\partial B,\mathbf{0}}(X_h;\mathbb{R}^d), \end{cases} \tag{15}$$

where $H^1_{\partial B,\mathbf{0}}(X;\mathbb{R}^d) := \{\boldsymbol{\varphi} \in H^1(X;\mathbb{R}^d) \mid \boldsymbol{\varphi} = \mathbf{0} \text{ on } \partial B\}$. Obviously, the integral equation in above equation can be evaluated even for $V_n\nu \in \mathbb{P}_0(\Gamma_h)$.

An algorithm following the above resolutions to solve Problem 1.1.1 with $\alpha = 1$, $g = 0$, $\lambda = 0$, and $\boldsymbol{\gamma} = \mathbf{0}$ is provided in [27, Algorithm 1, p. 981].

2. Mean curvature flow problem

2.1. Application of CMM to MCF

We will showcase in this short section how CMM is applied to solve MCF problems [7,13,14,16]. It could be argued that using the proposed scheme is somehow inappropriate to use for MCF problems since CMM not only discretizes the boundary, but the whole domain. We underline here that the discretization of the domain is not needed in numerically solving moving boundary problems whose movement is only influence by its geometric shape — at least when a different approach from FEM is employed. However, this section actually serves as a preparation for solving the one-phase quasi-stationary Stefan problem with Gibbs–Thomson law and kinetic undercooling which we will examine in detail in a follow-up investigation. For this reason, we will exhibit below the applicability of CMM to MCF problems.

Mean-curvature flow problems are typically described by the normal flow $V_n\nu$ with speed

$$V_n = -\kappa \quad \text{on } \Gamma(t), \tag{16}$$

where κ denotes the sum of principal curvatures of the moving surface $\Gamma(t)$ for $d \geqslant 3$. In 2D, of course, κ corresponds to the curvature of the moving boundary $\Gamma(t)$.

Given the normal speed $V_n = -\kappa$, the corresponding weak formulation of (14) can be stated as follows:

$$\begin{cases} \text{find } \mathbf{w} \in H^1(\Omega;\mathbb{R}^d) \text{ such that} \\ \quad a_{\Omega,\Gamma}(\mathbf{w},\boldsymbol{\varphi}) = -\dfrac{1}{\varepsilon}\displaystyle\int_\Gamma \mathrm{div}_\Gamma\, \boldsymbol{\varphi}\, ds, \quad \text{for all } \boldsymbol{\varphi} \in H^1(\Omega;\mathbb{R}^d), \end{cases} \tag{17}$$

where div_Γ denotes the *tangential divergence* (see, e.g., [18, Chap. 3, Sec. 1, Def. 2.3, p. 53]). The variational equation above was obtained via the *Gauss–Green formula* on Γ (see, e.g., [18, Chap. 2, Sec. 2, Thm. 2.18, p. 56]). Observe above that the equation does not require the explicit computation of κ which is an advantage of CMM.

The above idea is realized numerically with the help of the identity

$$\int_\Gamma \mathrm{div}_\Gamma\, \boldsymbol{\varphi}\, ds = \int_\Gamma \left(\mathrm{div}\,\boldsymbol{\varphi} - \frac{\partial\boldsymbol{\varphi}}{\partial\nu}\cdot\nu\right) ds;$$

see [27]. More precisely, we will apply CMM to the MCF problem by solving the following variational problem:

$$\begin{cases} \text{find } \mathbf{w}_h \in \mathbb{P}_1(\Omega_h;\mathbb{R}^d) \text{ such that} \\ \quad a_{\Omega_h,\Gamma_h}(\mathbf{w}_h,\boldsymbol{\varphi}_h) = -\dfrac{1}{\varepsilon}\displaystyle\int_{\Gamma_h} \left(\mathrm{div}\,\boldsymbol{\varphi}_h - \frac{\partial\boldsymbol{\varphi}_h}{\partial\nu}\cdot\nu\right) ds, \quad \forall\boldsymbol{\varphi}_h \in \mathbb{P}_1(\Omega_h;\mathbb{R}^d). \end{cases}$$

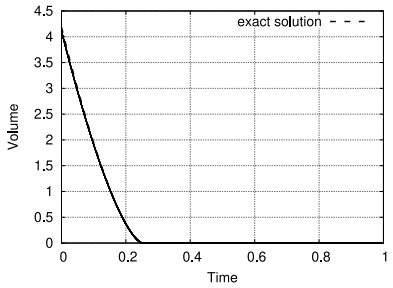

Fig. 1. Time variation of volume $|\Omega_h^k|$ for Example 1.

For the MCF problem, the CMM algorithm is formulated as follows:

Algorithm 1 CMM Algorithm for MCF

1: Set $T > 0$, $N_T \in \mathbb{N}$, $\varepsilon > 0$, $k = 0$, and generate $\overline{\Omega}_h^0 \approx \overline{\Omega}^0$.
2: **while** $k \leqslant N_T$ **do**
3: Compute $\mathbf{w}_h^k \in \mathbb{P}_1(\Omega_h^k; \mathbb{R}^d)$ by solving

$$a_{\Omega_h^k, \Gamma_h^k}(\mathbf{w}_h, \varphi_h) = -\frac{1}{\varepsilon} \int_{\Gamma_h^k} \left(\operatorname{div} \varphi_h - \frac{\partial \varphi_h}{\partial \nu} \cdot \nu \right) \, ds, \quad \forall \varphi_h \in \mathbb{P}_1(\Omega_h^k; \mathbb{R}^d).$$

4: Update the current domain by moving the mesh according to (11) and (12).
5: $k \leftarrow k + 1$
6: **end while**

2.2. Numerical examples

As the numerical investigation carried out in [27] was limited to two dimensional cases, we provide here two numerical examples in the case of three dimensions. The first one considers the case when the moving surface has an initial shape given by a sphere while the second one issues an example with a torus as the initial shape.

Numerical example 1. *We let* $\Omega^0 := \left\{ x \in \mathbb{R}^3 \mid |x| \leqslant 1 \right\}$ *and execute the scheme with parameter values* $\varepsilon = 0.01$, $\tau = 10^{-4}$, $h \approx 0.33$, *and* $T = 1$.

Numerical example 2. *We consider a torus with major radius* $R_0 = 2$ *and minor radius* $r_0 = 1$, *i.e., we let* $\Omega^0 := \{x \in \mathbb{R}^3 \mid (\sqrt{x_1^2 + x_2^2} - 2)^2 + x_3^2 \leqslant 1\}$. *For this experiment, we set* $\varepsilon = 0.1$, $\tau = 10^{-5}$, $h \approx 0.98$, *and* $T = 1$.

For the first test case, we note that a sphere of radius R has the mean curvature $\kappa = -(d-1)/R$. Because of the radial symmetry, we get the exact solution $R(t) = \sqrt{R_0^2 - 2(d-1)t}$ for $t \in (0, R_0^2/2(d-1))$ when the initial radius is $R_0 := R(0)$. The time variation of the volume $|\Omega_h^k|$ for this test example is plotted in Fig. 1. Evidently, the computed volume agrees with the volume of the true solution, and as expected, the sphere eventually vanishes in time.

On the other hand, the torus does not keep a circular cross-section under MCF because the curvature of the torus is greater on the outside of the hole away from the center. However, thin torus is known to shrink into a circular ring of singularities centered on the z-axis, and this has been confirmed numerically by the level-set method [3].

As expected, see Fig. 2(a) to Fig. 2(e), the surface area of the evolving domain decreases due to the mean curvature flow. We note, however, that unlike the sphere, no exact solution is known for the torus. Therefore, by assuming that the curvature flow depends only on the minor radius $r(t)$, the volume of the torus can be approximated as $|\Omega| \approx 2\pi^2 R_0 (r_0^2 - 2t)$ for $t \in (0, r_0^2/2)$. The time variation of the mesh volume $|\Omega_h^k|$, which is plotted in Fig. 2(f), closely agrees with the volume of the approximated solution.

3. Stefan problem

While the previous work [27] have dealt with quasi-stationary problems such as the Hele-Shaw problem and the curve shortening problem with CMM, this section will focus on the Stefan problem, one of the problems where the interior of the domain is also described by a time-evolution equation:

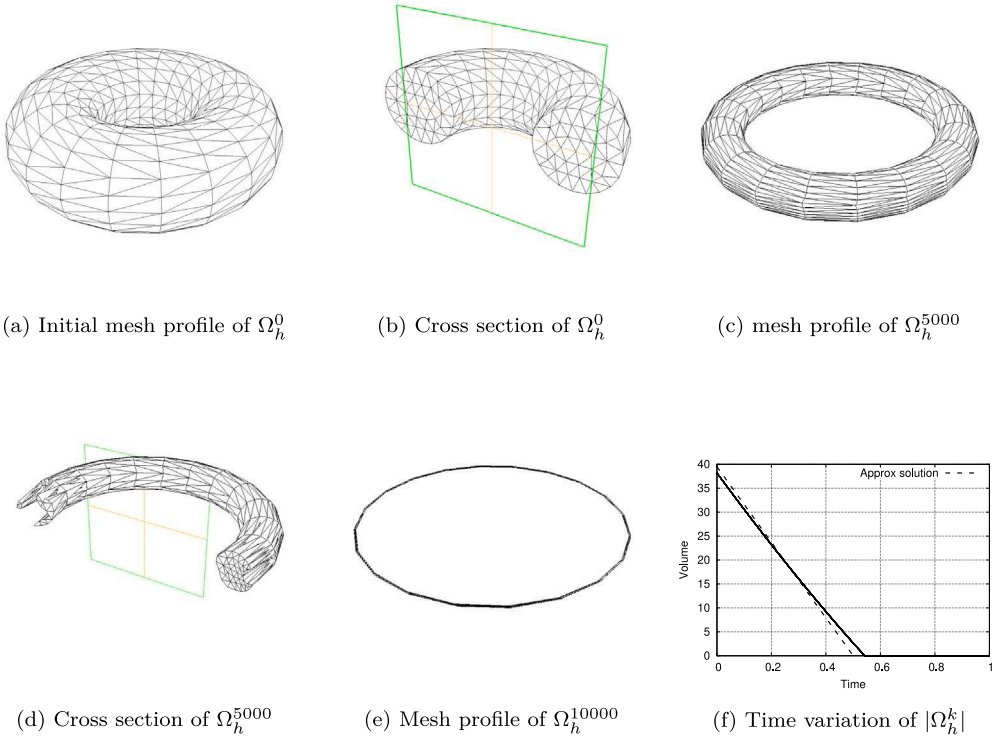

(a) Initial mesh profile of Ω_h^0 (b) Cross section of Ω_h^0 (c) mesh profile of Ω_h^{5000}

(d) Cross section of Ω_h^{5000} (e) Mesh profile of Ω_h^{10000} (f) Time variation of $|\Omega_h^k|$

Fig. 2. Computational results for Example 2.

Problem 3.0.1. Find $\Omega(t) \supset \overline{B}$ and $u(\cdot,\ t) : \overline{\Omega(t)} \setminus B \to \mathbb{R}$ such that

$$\begin{cases} \dfrac{\partial u}{\partial t} - \Delta u = f & \text{in } \Omega(t) \setminus \overline{B}, \quad t \in [0,T], \\ (1-\alpha)u + \alpha \dfrac{\partial u}{\partial \nu} = q_B & \text{on } \partial B, \\ u = 0 & \text{on } \Gamma(t), \quad t \in [0,T], \\ V_n = (-\nabla u + \gamma) \cdot \nu & \text{on } \Gamma(t), \quad t \in [0,T], \\ \Omega(0) = \Omega_0, & \\ u(\cdot,0) = u_0(\cdot) & \text{in } \Omega_0 \setminus \overline{B}, \end{cases} \tag{18}$$

where $f : \mathbb{R}^d \times [0,T] \to \mathbb{R}$, $q_B : \partial B \times [0,T] \to \mathbb{R}$, $\boldsymbol{\gamma} : \mathbb{R}^d \times [0,T] \to \mathbb{R}^d$ are given functions, Ω_0 is the initial profile of $\Omega(t)$, $u_0 : \Omega_0 \to \mathbb{R}$, and $V_n := V_n(x,t)$, $x \in \Gamma(t)$, describes the outward normal velocity of the moving interface $\Gamma(t)$. The constant $\alpha \in \{0,1\}$ dictates whether the fixed part accepts a Dirichlet or Neumann boundary condition.

The Stefan problem, introduced by Jožef Stefan in 1889, models the melting ice as a moving boundary problem. It involves the Stefan condition, which dictates the boundary's normal velocity proportional to the temperature gradient at the interface. These conditions are based on the Fourier law for heat conduction, Fick law for mass diffusion, and Darcy law for osmotic flow. When considering only one variable, like in (18), it becomes the one-phase Stefan problem. Analytical solutions are challenging to obtain, except for special cases like one-dimensional situations [22], leading to the active study of numerical methods. One such method is the level-set approach, which can handle various moving boundary problems, including topological changes [19]. Another method, the enthalpy formulation, employs enthalpy to convert the Stefan problem into a nonlinear diffusion equation containing implicit free boundary information [4,23]. The CMM is an explicit front tracking-type method that is advantageous due to easy implementation, extensibility to 3D problems, and avoidance of mesh regeneration at each time step during approximation. Therefore, exploring the application of CMM to non-stationary problems, such as the Stefan problem, becomes relevant.

Before we demonstrate the application of CMM to Stefan problems, we briefly offer insights into prior research on one/multi-phase Stefan/Hele-Shaw problems, with a focus on numerical aspects. Many of the relevant studies can be found and were reviewed in the work of Visintin [29] and in the references therein. Firstly, the nonlinear analytic semigroup approach for two-phase Stefan/Hele-Shaw problems, with or without curvature terms, allows one to prove the existence of a time-local classical solution. However, it does not help us consider a useful numerical scheme. Meanwhile, several weak formulations for two-phase Stefan/Hele-Shaw problems with/without curvature terms are known, and it is possible to consider numerical schemes based on weak formulations. Moreover, variational *inequality* formulations for one-phase Stefan/Hele-Shaw problems without curvature terms

are known, and it is possible to consider numerical schemes based on those formulations. However, to the best of our knowledge, no suitable weak formulations are known for one-phase Stefan/Hele-Shaw problems with curvature terms. Thus, finding satisfactory numerical solutions, especially for three-dimensional problems, remains an issue. The CMM, as proposed in this paper, addresses the above mentioned issues for solving one/multi-phase Stefan/Hele-Shaw problems.

3.1. Application of CMM to one-phase Stefan problems

In the following, we set $\alpha = 1$ for simplicity. Utilizing the same notation introduced in Section 1.3, a naive numerical method for Stefan problem using CMM consists of the following steps.

Conventional scheme for (18)

At each time $t = k\tau$, $k = 0, 1, 2, \ldots$, let Ω_h^k and u_h^k be given. The evolution of the domain is numerically solved by the following steps:

Step 1. First, define the normal velocity as $V_n^k := (-\nabla u_h^k + \gamma^k) \cdot \nu_h^k$ on Γ_h^k.

Step 2. Then, create an extension of $V_n^k \nu^k$ by solving the FE solution $\mathbf{w}_h^k \in \mathbb{P}_1(\Omega_h^k \setminus \overline{B}_h; \mathbb{R}^d)$ for the following:

$$\begin{cases} -\Delta \mathbf{w}_h^k = \mathbf{0} & \text{in } \Omega_h^k \setminus \overline{B}_h, \\ \mathbf{w}_h^k = \mathbf{0} & \text{on } \partial B_h, \\ \varepsilon \nabla \mathbf{w}_h^k \cdot \nu_h^k + \mathbf{w}_h^k = V_n^k \nu_h^k & \text{on } \Gamma_h^k. \end{cases}$$

Step 3. Next, update the current domain by moving the mesh according to

$$\overline{\Omega}_h^{k+1} \setminus B_h := \left\{ x + \tau \mathbf{w}_h^k(x) \;\middle|\; x \in \overline{\Omega}_h^k \setminus B_h \right\}.$$

Step 4. Finally, we solve the FE solution u_h^{k+1} over the domain $\Omega_h^{k+1} \setminus \overline{B}_h$:

$$\begin{cases} \boxed{\dfrac{\partial u}{\partial t}}^{k+1} - \Delta u^{k+1} = f^{k+1} & \text{in } \Omega_h^{k+1} \setminus \overline{B}_h, \\ \nabla u^{k+1} \cdot \nu^{k+1} = q_B^{k+1} & \text{on } \partial B_h, \\ u^{k+1} = 0 & \text{on } \Gamma_h^{k+1}. \end{cases} \tag{19}$$

Recall that CMM is an alternative solution procedure that breaks down the quasi-stationary moving boundary problem into two steps. First, it tackles the boundary value problem in a fixed domain. Second, it updates the mesh by employing harmonic expansion of the given normal velocity. In order to solve the time-evolution equation using a simple difference approximation with the non-stationary term as $(u_h^{k+1} - u_h^k)/\tau$, we require the knowledge of the previous information u_h^k in the updated mesh Ω_h^{k+1}.

A straightforward approach to address this issue is to extend the values of u_h^k from Ω_h^k to Ω_h^{k+1} via interpolation. Alternatively, since CMM follows a Lagrangian approach with a Laplacian vector field, the non-stationary terms can be expressed in terms of the material derivative.

In this study, we propose an Arbitrary Lagrangian-Eulerian (ALE) method that employs the material derivative and the Galerkin method of characteristics [28]. The Galerkin method of characteristics is recognized as an effective approach for solving convection problems. It is worth noting that, unlike the original Galerkin method of characteristics, in the numerical procedure that we propose below, the advection term is retained instead of being handled solely by the material derivative. Nevertheless, this approach offers the advantage of enabling CMM to be applied to non-stationary problems with a non-zero Dirichlet condition $u \not\equiv 0$ on Γ.

Given a flow velocity field $\tilde{\mathbf{w}}$, the material derivative (or Lagrangian derivative) Du/Dt is defined as follows:

$$\frac{Du}{Dt} := \frac{\partial u}{\partial t} + \tilde{\mathbf{w}} \cdot \nabla u. \tag{20}$$

For clarity, let us briefly review the method of characteristics. If $X : (0, T] \to \mathbb{R}^d$ is a solution to the ordinary differential equation (ODE)

$$\frac{dX}{dt}(t) = \tilde{\mathbf{w}}(X(t), t),$$

where $X(t)$ is the characteristic curve, then (20) can be described as

$$\frac{d}{dt} u(X(t), t) = \frac{\partial u}{\partial t}(X(t), t) + \nabla u(X(t), t) \cdot \frac{dX}{dt}(t) = \frac{\partial u}{\partial t}(X(t), t) + \nabla u(X(t), t) \cdot \tilde{\mathbf{w}}(X(t), t) = \frac{Du}{Dt}(X(t), t). \tag{21}$$

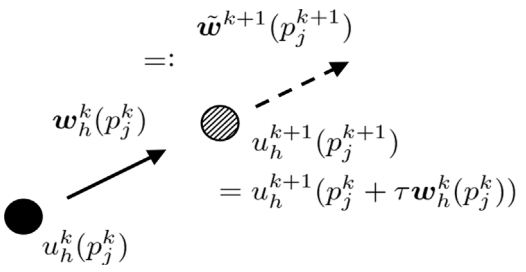

Fig. 3. Setting the advection $\tilde{\mathbf{w}}^{k+1}$.

The symbols used for discretization are used as they are from the previous subsections. Approximating the left side of (21) by the backward-Euler method, one obtains the following equation:

$$\frac{Du}{Dt}(X(t),t) \approx \frac{u(X(t),t) - u(X(t-\tau),t-\tau)}{\tau}. \tag{22}$$

Subject to an initial condition $X(t) = x_t$, we get an approximation of X at $t - \tau$:

$$X(t-\tau) \approx x_t - \tau \tilde{\mathbf{w}}(x_t,t) =: X_1(x_t). \tag{23}$$

Hereinafter, we consider the application of method of characteristics to CMM. Using the material derivative (20), the heat equation can be rewritten as

$$\frac{Du}{Dt} - \tilde{\mathbf{w}} \cdot \nabla u - \Delta u = f. \tag{24}$$

Therefore, (19) is time-discretized by (22), (23), and (24),

$$\begin{cases} \dfrac{u^{k+1} - u^k \circ X_1^{k+1}}{\tau} - \tilde{\mathbf{w}}^{k+1} \cdot \nabla u^{k+1} - \Delta u^{k+1} = f^{k+1} & \text{in } \Omega_h^{k+1} \setminus \overline{B}_h, \\ \nabla u^{k+1} \cdot \nu^{k+1} = q_B^{k+1} & \text{on } \partial B_h, \\ u^{k+1} = 0 & \text{on } \Gamma^{k+1}, \end{cases} \tag{25}$$

where $X_1^{k+1}(x) := x - \tau \tilde{\mathbf{w}}^{k+1}(x)$ for $x \in \Omega_h^{k+1}$. However, given the above system of equations, two issues emerge: (i) the calculation of the advection term $\tilde{\mathbf{w}}^{k+1} \cdot \nabla u^{k+1}$ for unknown $\tilde{\mathbf{w}}^{k+1}$, and (ii) the exact definition of $\tilde{\mathbf{w}}$.

To address this issues, we suggest simply reusing $\mathbf{w}_h^k$ as $\tilde{\mathbf{w}}^{k+1}$. More precisely, let the triangular mesh be $\mathcal{T}_h(\overline{\Omega}_h^k \setminus B_h)$ with the set of nodal points $\mathcal{N}_h^k = \{p_j^k\}_{j=1}^{N_p}$. For $p_j^{k+1} := p_j^k + \tau \mathbf{w}_h^k(p_j^k)$, we set (see Fig. 3 for illustration)

$$\tilde{\mathbf{w}}^{k+1}(p_j^{k+1}) := \mathbf{w}_h^k(p_j^k) \quad \text{for all } j = 1, \dots, N_p. \tag{26}$$

By doing so, $u_h^k \circ X_1^{k+1}$ is known, and $\tilde{\mathbf{w}}^{k+1} \cdot \nabla u^{k+1}$ can easily be calculated for all nodal points. The advantage of defining (26) is that at least the material derivative can be calculated correctly. Thus, all we have to do now is solve the weak formulation of (25) numerically: find $u_h^{k+1} \in H^1_{\Gamma_h^{k+1},0}(\Omega_h^{k+1} \setminus \overline{B}_h)$ such that

$$\begin{aligned} &\int_{\Omega_h^{k+1} \setminus \overline{B}_h} \left(\frac{u_h^{k+1} - u_h^k \circ X_1^{k+1}}{\tau} \right) \varphi_h \, dx - \int_{\Omega_h^{k+1} \setminus \overline{B}_h} (\nabla u_h^{k+1} \cdot \tilde{\mathbf{w}}^{k+1}) \varphi_h \, dx \\ &\quad + \int_{\Omega_h^{k+1} \setminus \overline{B}_h} \nabla u_h^{k+1} \cdot \nabla \varphi_h \, dx - \int_{\partial B_h} q_B^{k+1} \varphi_h \, ds - \int_{\Omega_h^{k+1} \setminus \overline{B}_h} f^{k+1} \varphi_h \, dx \\ &\quad = 0, \qquad \text{for all } \varphi_h \in H^1_{\Gamma_h^{k+1},0}(\Omega_h^{k+1} \setminus \overline{B}_h). \end{aligned} \tag{27}$$

The above schemes is summarized in Algorithm 2.

Algorithm 2 CMM for the one-phase Stefan problem

1: Specify $T > 0$, $N_T \in \mathbb{N}$, $\varepsilon > 0$, and set $k = 0$. Also, generate a finite element mesh of the initial domain $\overline{\Omega}_h^0 \approx \overline{\Omega}^0$, and let $u_h^0 \approx u_0$ be given.
2: **while** $k \leqslant N_T$ **do**
3: Define the normal velocity as $V_n^k := (-\nabla u_h^k + \gamma^k) \cdot \nu^k$ on Γ_h^k.
4: Create an extension of $V_n^k \nu^k$ by solving the finite element solution $\mathbf{w}_h^k \in \mathbb{P}_1(\Omega_h^k; \mathbb{R}^d)$ of the following system PDEs:

$$-\Delta \mathbf{w}^k = \mathbf{0} \ \text{ in } \Omega_h^k, \quad \mathbf{w}^k = \mathbf{0} \ \text{ on } \partial B_h, \quad \varepsilon \nabla \mathbf{w}^k \cdot \nu^k + \mathbf{w}^k = V_n^k \nu^k \ \text{ on } \Gamma_h^k.$$

5: Update the current domain by moving the mesh according to the following:

$$\overline{\Omega}_h^{k+1} \setminus B_h := \left\{ x + \tau \mathbf{w}_h^k(x) \;\middle|\; x \in \overline{\Omega}_h^k \setminus B_h \right\}.$$

6: Solve the finite element solution $u_h^{k+1} \in \mathbb{P}_1(\Omega_h^{k+1})$ for the following:

$$\begin{cases} \dfrac{u^{k+1} - u^k \circ X_1^{k+1}}{\tau} - \tilde{\mathbf{w}}^{k+1} \cdot \nabla u^{k+1} - \Delta u^{k+1} = f^{k+1} & \text{in } \Omega_h^{k+1} \setminus \overline{B}_h, \\ \nabla u^{k+1} \cdot \nu^{k+1} = q_B^{k+1} & \text{on } \partial B_h, \\ u^{k+1} = 0 & \text{on } \Gamma^{k+1}. \end{cases} \tag{28}$$

or

$$\begin{cases} \dfrac{u^{k+1} - \tilde{u}^k}{\tau} - \Delta u^{k+1} = f^{k+1} & \text{in } \Omega_h^{k+1} \setminus \overline{B}_h, \\ \nabla u^{k+1} \cdot \nu^{k+1} = q_B^{k+1} & \text{on } \partial B_h, \\ u^{k+1} = 0 & \text{on } \Gamma^{k+1}, \end{cases} \tag{29}$$

where $X_1^{k+1}(x) := x - \tau \tilde{\mathbf{w}}^{k+1}(x)$ for $x \in \Omega_h^{k+1}$, $\tilde{\mathbf{w}}^{k+1}(p_j^{k+1}) := \mathbf{w}_h^k(p_j^k)$, $j = 1, \cdots, N_p$, and $\tilde{u}^k \in \Omega_h^{k+1}$ is the zero-extension of u_h^k.
7: $k \leftarrow k + 1$
8: **end while**

Remark 3.1.1. We emphasize that the proposed numerical method is not limited to one-phase problems, but is also applicable to two-phase and more general multi-phase Stefan problems. The comoving mesh method introduced in this study is independent of the number of phases present in the physical problem described by the evolution equation. As the internal nodes of the mesh discretization move simultaneously with the nodes on the moving boundary, the interface boundary adjusts according to the interface velocity of the associated ε-regularized moving interface/boundary problem. Therefore, extending the method to multi-phase Stefan problems poses no difficulty.

3.2. A numerical example for the classical Stefan problem

In the following, we present a numerical example of the classical Stefan problem:

$$\begin{cases} \dfrac{\partial u}{\partial t} - \Delta u = 0 & \text{in } \Omega(t) \setminus \overline{B}, \quad t \in [0, T], \\ \nabla u \cdot \nu = 1 & \text{on } \partial B, \\ u = 0 & \text{on } \Gamma(t), \quad t \in [0, T], \\ V_n = -\nabla u \cdot \nu & \text{on } \Gamma(t), \quad t \in [0, T], \\ \Omega(0) = \Omega_0 & \\ u(\cdot, 0) = 1 & \text{in } \Omega(0) \setminus \overline{B}. \end{cases} \tag{30}$$

Note that, because of the maximum principle, u is positive in $\Omega(t) \setminus \overline{B}$. This means that $\nabla u \cdot \nu < 0$ on the moving boundary, and, in this case, since the normal velocity V_n is always positive, the hypersurface expands.

Numerical example 3. *In this example, the initial profile is given as an hypotrochoid:*

$$\Omega_0 := \left\{ (r, \theta) \in \mathbb{R}^2 \;\middle|\; 0 \leqslant r^2 < \frac{(m-1)^2 + s^2 + 2(m-1)s\cos(m\theta)}{m^2}, \theta \in [0, 2\pi] \right\},$$

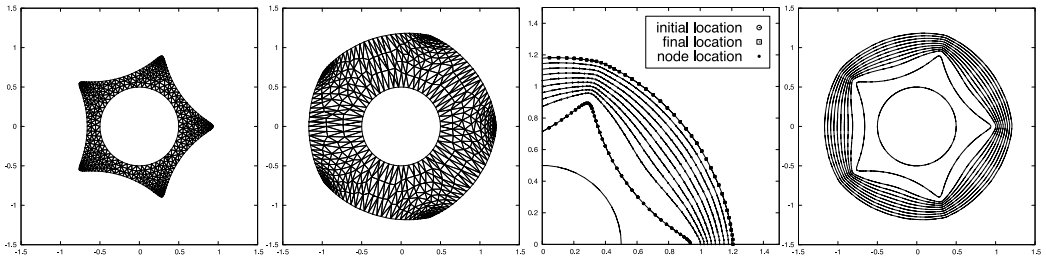

(a) Mesh at $T = 0$ (b) Mesh at $T = 1$ (c) Nodes trajectory (d) Shape evolution

Fig. 4. Computational results of Example 3.

with $m = 5$ and $s = 0.7$. Moreover, $\overline{B}$ is the circle $C(\mathbf{0}, 0.5)$ as shown in Fig. 4(a), and the final time is set to $T = 1$. Algorithm 2 is executed using mesh sizes of uniform width $h \approx 0.085$ with parameter value $\varepsilon = 0.1$ and time step size $\tau = 0.01$. Fig. 4 summarizes the mesh profile at the initial and final times, along with the trajectory nodes and the evolution of the shape.

3.3. EOC for the moving boundary diffusion problem

Before checking the EOC of the Stefan problem, we consider the following moving boundary diffusion problem for the purpose of checking the accuracy of the non-stationary terms.

Problem 3.3.1. Suppose $\phi(x,t)$ is a smooth function with $|\nabla\phi| \neq 0$ on $\{\phi = 0\}$ for $t \in [0,T]$. For a given $\Omega(t) := \{x \in \mathbb{R}^d \mid \phi(x,t) < 0\}$, $f, g : \mathbb{R}^d \times [0,T] \to \mathbb{R}$, and $u_0 : \mathbb{R}^d \to \mathbb{R}$, find $u(\cdot, t) : \overline{\Omega(t)} \to \mathbb{R}$ such that

$$\begin{cases} \dfrac{\partial u}{\partial t} - \Delta u = f & \text{in } \Omega(t), \quad t \in (0,T], \\ u = g & \text{on } \Gamma(t) := \partial\Omega(t), \quad t \in (0,T], \\ u(\cdot,0) = u_0(\cdot) & \text{in } \Omega(0), \end{cases} \tag{31}$$

We state the following construction of the appropriate manufactured solution.

Proposition 3.3.1. *We define $f := -\dfrac{\partial\phi}{\partial t} + \Delta\phi$, $g := 0$. Then, $u = -\phi$ is the solution of (31).*

Proof. The proposition easily follows from straightforward computation of V_n with the normal vector ν computed via the level-set function ϕ. □

We now examine the EOC of the scheme using Proposition 3.3.1 and the following numerical errors

$$\mathrm{err}_{\mathcal{X}^k} := \max_{0 \leqslant k \leqslant N_T} \left\{ \left\| u_h^k - \Pi_h u(\cdot, k\tau) \right\|_{\mathcal{X}^k} \right\}, \qquad \mathcal{X}^k \in \{L^2(\Omega_h^k), H^1(\Omega_h^k)\}.$$

Numerical example 4. *As an example, we perform a numerical experiment with the following conditions: $\varepsilon \in \{10^{-4}, 10^{-1}\}$, $h \approx \tau$,*

$$\phi(x,t) := \frac{x_1^2}{2(t+1)} + \frac{x_2^2}{t+1} - 1, \quad t \in [0,1], \quad (x := (x_1, x_2)).$$

Therefore, the solution domain $\Omega(t) = \left\{ x \in \mathbb{R}^2 \;\middle|\; 0.5x_1^2 + x_2^2 < t+1 \right\}$ is an elliptical shape whose area is expanding through time. Fig. 5 summarizes the error of convergences with respect to the L^2 and H^1 norms.

Numerical example 5. *In the previous example, we discussed an example in which the area expands, whereas in this numerical example, the area of the region does not change, but rather moves in a parallel direction: $\varepsilon \in \{10^{-4}, 10^{-1}\}$, $h \approx \tau$,*

$$\phi(x,t) := 0.5(x_1 - t)^2 + (x_2 - t)^2 - 1, \quad t \in [0,1], \quad (x := (x_1, x_2)),$$

so $\Omega(t) = \left\{ x \in \mathbb{R}^2 \;\middle|\; 0.5(x_1 - t)^2 + (x_2 - t)^2 < 1, \right\}$.

To check the accuracy of the discretization of the nonstationary terms, two numerical experimental examples diffusion-ellipse and ith known moving boundaries were performed. Then, when the parameter ε is sufficiently small, EOC is approximately first order, and convergence is expected for both numerical examples. Furthermore, comparing ALE method (Figs. 6(a)–6(b)) and zero-extension (Figs. 6(c)–6(d)), the error trends appear almost identical. One reason is that both are discretized in time using backward Euler method, which is a first-order numerical procedure.

Algorithm 3 CMM for the moving boundary diffusion problem

1: Specify $T > 0$, $N_T \in \mathbb{N}$, $\varepsilon > 0$, and set $k = 0$. Also, generate a finite element mesh of the initial domain $\overline{\Omega}_h^0 \approx \overline{\Omega}^0$, and let $u_h^0 \approx u_0$ be given.
2: **while** $k \leqslant N_T$ **do**
3: Define the normal velocity as $V_n^k := \phi_t/|\nabla\phi|$ on Γ_h^k.
4: Create an extension of $V_n^k \nu^k$ by solving the finite element solution $\mathbf{w}_h^k \in \mathbb{P}_1(\Omega_h^k; \mathbb{R}^d)$ for the following:

$$-\Delta \mathbf{w}^k = \mathbf{0} \ \text{ in } \Omega_h^k, \quad \varepsilon \nabla \mathbf{w}^k \cdot \nu^k + \mathbf{w}^k = V_n^k \nu^k \ \text{ on } \Gamma_h^k.$$

5: Update the current domain by moving the mesh according to

$$\overline{\Omega_h^{k+1}} := \left\{ x + \tau \mathbf{w}_h^k(x) \;\middle|\; x \in \overline{\Omega_h^k} \right\}, \quad \text{where } \tau = T/N_T.$$

6: Solve the finite element solution $u_h^{k+1} \in \mathbb{P}_1(\Omega_h^{k+1})$ for the following:

$$\begin{cases} \dfrac{u^{k+1} - u^k \circ X_1^{k+1}}{\tau} - \tilde{\mathbf{w}}^{k+1} \cdot \nabla u^{k+1} - \Delta u^{k+1} = f^{k+1} & \text{in } \Omega_h^{k+1}, \\ u^{k+1} = 0 & \text{on } \Gamma^{k+1}. \end{cases} \tag{32}$$

or

$$\frac{u^{k+1} - \tilde{u}^k}{\tau} - \Delta u^{k+1} = f^{k+1} \quad \text{in } \Omega_h^{k+1}, \qquad u^{k+1} = 0 \quad \text{on } \Gamma_h^{k+1}, \tag{33}$$

where $X_1^{k+1}(x) := x - \tau \tilde{\mathbf{w}}^{k+1}(x)$ for $x \in \Omega_h^{k+1}$, $\tilde{\mathbf{w}}^{k+1}(p_j^{k+1}) := \mathbf{w}_h^k(p_j^k)$, $j = 1, \cdots, N_p$, and $\tilde{u}^k \in \Omega_h^{k+1}$ is the zero-extension of u_h^k.
7: $k \leftarrow k + 1$
8: **end while**

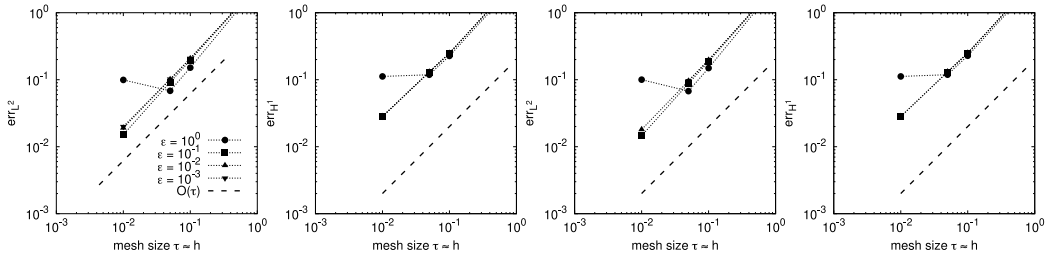

(a) τ vs err_{L^2} for (32) (b) τ vs err_{H^1} for (32) (c) τ vs err_{L^2} for (33) (d) ε vs err_{H^1} for (33)

Fig. 5. Error of convergences for *Example 4*.

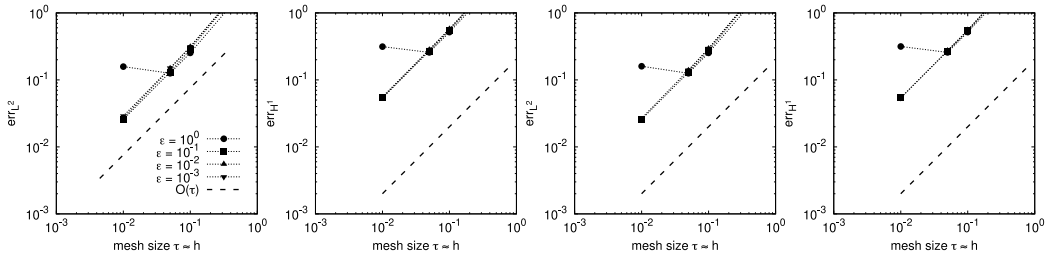

(a) τ vs err_{L^2} for (32) (b) τ vs err_{H^1} for (32) (c) τ vs err_{L^2} for (33) (d) ε vs err_{H^1} for (33)

Fig. 6. Error of convergences for Example 5.

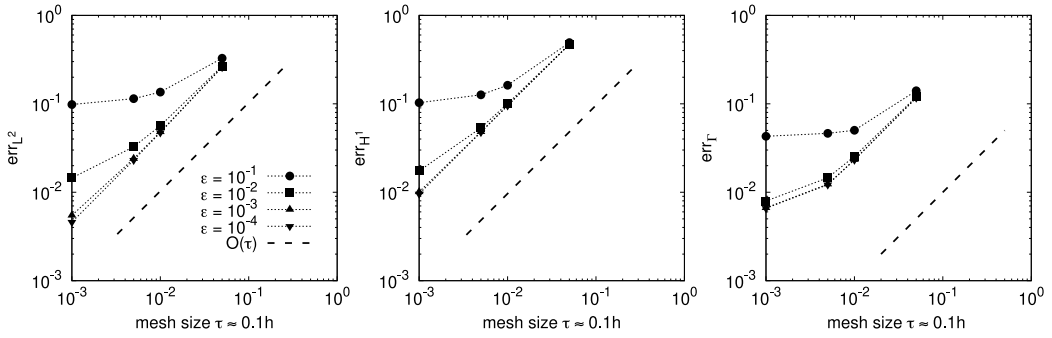

(a) τ vs err_{L^2} for (28) (b) τ vs err_{H^1} for (28) (c) τ vs err_{Γ} for (28)

Fig. 7. Error of convergences for Example 6 (ALE method).

3.4. EOC for the Stefan problem

We will check the accuracy of CMM for the Stefan problem (18). On this purpose, we state the following construction of the appropriate manufactured solution.

Proposition 3.4.1. *We set* $\alpha = 1$ *and define* $f := -\frac{\partial \phi}{\partial t} + \Delta\phi$, $q_B := -\nabla\phi \cdot \nu$, $\gamma := \left(-\frac{\phi_t}{|\nabla\phi|^2} - 1\right)\nabla\phi$, $\Omega_0 := \{\phi(x,0) < 0\}$. *Then,* $u = -\phi$ *and* $\Omega(t) := \{x \in \mathbb{R}^d \mid \phi(x,t) < 0\}$ *are the solutions of* (18).

Proof. The proposition readily follows from a straightforward computation of V_n using the normal vector ν calculated via the level-set function ϕ. □

We now examine the EOC of the scheme using Proposition 3.4.1. With regards to EOC, we define the numerical errors as follows:

$$\mathrm{err}_{\Gamma} := \max_{0\leqslant k\leqslant N_T} \max_{x\in\Gamma_h^k} \mathrm{dist}(x, \Gamma(k\tau)), \qquad \mathrm{err}_{\mathcal{X}^k} := \max_{0\leqslant k\leqslant N_T} \left\{ \left\| u_h^k - \Pi_h u(\cdot, k\tau) \right\|_{\mathcal{X}^k} \right\},$$

where $\mathcal{X}^k \in \{L^2(\Omega_h^k), H^1(\Omega_h^k)\}$, and $\Pi_h : H^1(\Omega) \to \mathbb{P}_1(\mathcal{T}_h(\Omega))$ is the projection map such that $\Pi_h u(p) = u(p)$ for all nodal points $p \in \mathcal{N}_h$ of $\mathcal{T}_h(\Omega)$.

Numerical example 6. *As an example, we perform a numerical experiment with the following conditions:* $\varepsilon \in \{10^{-4}, 10^{-1}\}$, $h \approx 10\tau$,

$$\phi(x,t) := \frac{x_1^2}{2(t+1)} + \frac{x_2^2}{t+1} - 1, \quad t \in [0,1], \quad (x := (x_1, x_2)),$$

so the fixed domain is given by the set $\overline{B} := \left\{ x \in \mathbb{R}^2 \;\middle|\; x_1^2 + x_2^2 \leqslant 0.5^2 \right\}$, *while the evolving domain is given by* $\Omega(t) = \left\{ x \in \mathbb{R}^2 \;\middle|\; 0.5x_1^2 + x_2^2 < t + 1 \right\}$.

The EOC of the CMM for the Stefan problem is shown in comparison with the ALE method (Fig. 7) and interpolation at the previous nodes (Fig. 8). As with the moving boundary diffusion problem, the order of convergence for both methods with respect to the L^2 and H^1 error is first order when ε is sufficiently small, and there is not much difference. The shape error graphs were also similar to those obtained in numerical experiments for the Hele-Shaw problem issued in [27].

4. Extensions by linear elasticity equation

In this section, let us consider the extension of $V_n\nu$ by a linear elasticity equation instead of the harmonic extension used in (14). Such choice of extension has been first considered in [1] and was called the *traction method* in the context of shape optimization.

Let us again consider our computational domain to have an interior (i.e., $B \neq \emptyset$) and exterior boundary ∂B and Γ, respectively. For CMM with the linear elasticity equation, the interior and boundary nodes of the mesh are moved simultaneously by the displacement vector $\mathbf{w}$ satisfying

$$\begin{cases} -\operatorname{div}\boldsymbol{\sigma}(\mathbf{w}) = \mathbf{0} & \text{in } \Omega \setminus \overline{B}, \\ \mathbf{w} = \mathbf{0} & \text{on } \partial B, \\ \mathbf{w} = V_n\nu & \text{on } \Gamma, \end{cases} \tag{34}$$

where $\boldsymbol{\sigma}(\mathbf{w}) \in \mathbb{R}^{d\times d}$ is the stress tensor and satisfies Hooke's law; i.e., $\boldsymbol{\sigma}(\mathbf{w}) = \mathbf{C}\mathbf{e}(\mathbf{w})$ where $\mathbf{C} \in \mathbb{R}^{d\times d\times d\times d}$ is the elasticity tensor (for isotropic linear elastic materials) and $\mathbf{e}(\mathbf{w}) \in \mathbb{R}^{d\times d}$ is the strain tensor. Using the strain–displacement equation $\mathbf{e}(\mathbf{w}) = \frac{1}{2}(\nabla\mathbf{w} + (\nabla\mathbf{w})^\top)$

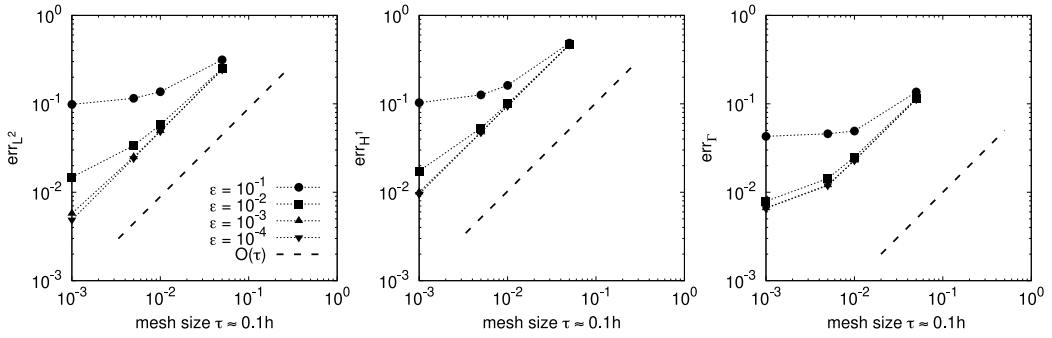

(a) τ vs err_{L^2} for (29) (b) τ vs err_{H^1} for (29) (c) τ vs err_{Γ} for (29)

Fig. 8. Error of convergences for Example 6 (zero-extension).

and the definition of the tensor $\mathbf{C}_{ijkl} = \lambda\delta_{ij}\delta_{kl} + \mu(\delta_{ik}\delta_{jl} + \delta_{il}\delta_{jk})$, where λ and μ are the Lamé constants, we can write $\boldsymbol{\sigma}(\mathbf{w}) = (\lambda(\operatorname{div}\mathbf{w}))I + 2\mu\mathbf{e}(\mathbf{w})$.

In the following, for simplicity, we will omit the number of iterations k, and furthermore, we will collectively set the boundary conditions for the boundary of $X = \Omega \setminus \overline{B}$ as follows:

$$\mathbf{g} := \begin{cases} \mathbf{0} & \text{on } \partial B, \\ V_n \nu & \text{on } \Gamma. \end{cases}$$

Using Gauss–Green's formula for sufficiently smooth matrix A and vector $\mathbf{v}$:

$$\int_\Omega -\operatorname{div} A \cdot \mathbf{v}\, dx = \int_\Omega A : \nabla\mathbf{v}\, dx - \int_\Gamma (A\nu)\cdot\mathbf{v}\, ds,$$

the weak form of system (34) is given as follows: find $\mathbf{w} \in H^1(X;\mathbb{R}^d)$ with $\mathbf{w} = \mathbf{g}$ on ∂X such that

$$\int_X [\lambda(\operatorname{div}\mathbf{w})(\operatorname{div}\boldsymbol{\varphi}) + 2\mu\mathbf{e}(\mathbf{w}) : \mathbf{e}(\boldsymbol{\varphi})]\, dx = 0, \quad \forall\boldsymbol{\varphi} \in H_0^1(X;\mathbb{R}^d). \tag{35}$$

The weak solution of (35) uniquely exists and satisfies the following variational principle (see, e.g. [6, Sec. 3, Chap. 4]):

$$\mathbf{w} = \underset{\substack{\mathbf{v}\in H^1(X;\mathbb{R}^d) \\ \mathbf{v}=\mathbf{g} \text{ on } \partial X}}{\arg\min}\ E(\mathbf{v}), \qquad E(\mathbf{v}) := \int_X \left[\lambda(div\mathbf{v})^2 + 2\mu|\mathbf{e}(\mathbf{v})|^2\right] dx. \tag{36}$$

On the other hand, we introduce the deviatoric strain tensor

$$\tilde{\mathbf{e}}(\mathbf{w}) := \mathbf{e}(\mathbf{w}) - \frac{\operatorname{div}\mathbf{w}}{d} I,$$

which is the strain tensor minus the mean strain. Using the equations

$$\tilde{\mathbf{e}}(\mathbf{w}) : I = \operatorname{tr}(\mathbf{e}(\mathbf{w})) - \frac{\operatorname{div}\mathbf{w}}{d}|I|^2 = \operatorname{tr}(\mathbf{e}(\mathbf{w})) - \frac{\operatorname{tr}(\mathbf{e}(\mathbf{w}))}{d} d = 0$$

and

$$\mathbf{e}(\mathbf{w}) : \mathbf{e}(\mathbf{v}) = \left(\tilde{\mathbf{e}}(\mathbf{w}) + \frac{\operatorname{div}\mathbf{w}}{d} I\right) : \left(\tilde{\mathbf{e}}(\mathbf{v}) + \frac{\operatorname{div}\mathbf{v}}{d} I\right) = \tilde{\mathbf{e}}(\mathbf{w}) : \tilde{\mathbf{e}}(\mathbf{v}) + \frac{(\operatorname{div}\mathbf{w})(\operatorname{div}\mathbf{v})}{d},$$

we can rewrite (36) using the deviatoric strain tensor as follows:

$$E(\mathbf{v}) = \left(\lambda + \frac{2\mu}{d}\right)\int_X (\operatorname{div}\mathbf{v})^2\, dx + 2\mu\int_X |\tilde{\mathbf{e}}(\mathbf{v})|^2\, dx =: \left(\lambda + \frac{2\mu}{d}\right) E_{\mathrm{iso}} + 2\mu E_{\mathrm{dev}}. \tag{37}$$

Note that Eq. (37) is divided into terms E_{iso} and E_{dev} representing volume change and shape change respectively.

Here, it is known that in the finite element method, the ratio of the diameters of the inscribed and circumscribed circles, called the aspect ratio $\sigma_K = h_K/\rho_K$, affects the local interpolation error in each element K (see, [9, Chap. 1.5]):

$$|u - \Pi_h u|_{1,2,K} \leqslant C h_K \sigma_K\, |u|_{2,2,K}, \quad \forall u \in H_0^1(K). \tag{38}$$

where $|u|_{s,p,K} := \sum_{|\alpha|=s} \|\partial^\alpha u\|_{L^p(K)}$ is a semi-norm in $W^{s,p}(K)$, ρ_K and h_K are the diameters of the inscribed and circumscribed circles, respectively. Therefore, only E_{dev} needs to be considered, since the quality of the mesh should not change even if E_{iso}, which represents isotropic deformation, is large. To see the relationship between shape change and deviatoric part E_{dev}, we calculate E_{dev} for similarity transformation (translation and rotation) and non-similarity transformation (scaling and shearing):

Example 4.0.1. We consider the affine map $\boldsymbol{\Phi} : x \mapsto Ax + \mathbf{b}$ where $A \in \mathbb{R}^{d\times d}$ and $\mathbf{b} \in \mathbb{R}^d$. Then, the displacement vector $\mathbf{v}$ is given by $\mathbf{v}(x) = \boldsymbol{\Phi}(x) - x = (A - I)x + \mathbf{b}$, and

$$E_{\mathrm{dev}} = \int_X |\tilde{\mathbf{e}}(\mathbf{v})|^2 \, dx = \int_X \left[|\mathbf{e}(\mathbf{v})|^2 - \frac{1}{d} \operatorname{tr}(\mathbf{e}(\mathbf{v}))^2 \right] dx = \int_X \left[\left| \frac{1}{2}(A + A^\top) - I \right|^2 - \frac{1}{d} (\operatorname{tr}(A) - d)^2 \right] dx.$$

First we consider the similarity transformation. In the translation case $\boldsymbol{\Phi}(x) := Ix + \mathbf{b}$, ($\mathbf{b} \in \mathbb{R}^d$), clearly

$$E_{\mathrm{dev}} = \int_X \left[\left| \frac{1}{2}(A + A^\top) - I \right|^2 - \frac{1}{d} (\operatorname{tr}(A) - d)^2 \right] dx = 0.$$

Also, for the 2D-rotation case $\boldsymbol{\Phi}(x) = Ax$, where

$$A = \begin{pmatrix} \cos\theta & -\sin\theta \\ \sin\theta & \cos\theta \end{pmatrix}, \quad \theta \in (0, 2\pi),$$

we have

$$\left| \frac{1}{2}(A + A^\top) - I \right|^2 = 2(\cos\theta - 1)^2, \quad \operatorname{tr} A = 2\cos\theta.$$

Therefore, we have

$$E_{\mathrm{dev}} = \int_X \left[\left| \frac{1}{2}(A + A^\top) - I \right|^2 - \frac{1}{2^2} (\operatorname{tr}(A) - d)^2 \right] dx = \int_X \left[2(\cos\theta - 1)^2 - \frac{1}{2}(2\cos\theta - 2)^2 \right] dx = 0.$$

On the other hand, E_{dev} is not 0 for the non-similarity transformation. In fact, for the shearing in y-axis case $\boldsymbol{\Phi}(x) = Ax$, where

$$A = \begin{pmatrix} 1 & s_x \\ 0 & 1 \end{pmatrix}, \quad s_x \in \mathbb{R},$$

we have

$$\left| \frac{1}{2}(A + A^\top) - I \right|^2 = \frac{s_x^2}{2}, \quad \operatorname{tr} A = d.$$

Therefore, for $s_x \neq 0$, we get

$$E_{\mathrm{dev}} = \int_X \left[\left| \frac{1}{2}(A + A^\top) - I \right|^2 - \frac{1}{2^2} (\operatorname{tr}(A) - d)^2 \right] dx = \int_X \frac{s_x^2}{2} \, dx > 0.$$

Furthermore, for the scaling case $\boldsymbol{\Phi}(x) := Ax$, where $A = \begin{pmatrix} a_x & 0 \\ 0 & a_y \end{pmatrix}$, a_x, $a_y \in \mathbb{R}$, we have

$$E_{\mathrm{dev}} = \int_X \left[\left| \frac{1}{2}(A + A^\top) - I \right|^2 - \frac{1}{d} (\operatorname{tr}(A) - d)^2 \right] dx = \int_X \frac{1}{2} \left| a_x - a_y \right|^2 \, dx \geqslant 0.$$

The equal sign is valid only if the aspect ratio is fixed, i.e. $a_x = a_y$.

Based on above discussion, the following results pertaining to mesh quality obtained via linear elasticity equation, especially in two dimensions, can easily be proved.

Proposition 4.0.1. *Let X be a bounded domain in $\mathbb{R}^2$. We suppose $\mathbf{w} \in H^1(X; \mathbb{R}^2)$. Then, the equation $-\Delta \mathbf{w} = 0$ in $\mathscr{D}'(X)$ is equivalent to the variational equation*

$$\int_X \tilde{\mathbf{e}}(\mathbf{w}) : \tilde{\mathbf{e}}(\boldsymbol{\varphi}) \, dx = 0, \ \forall \boldsymbol{\varphi} \in H_{\mathbf{0}}^1(X; \mathbb{R}^2).$$

Proof. We introduce the notation $\partial_i w_j := \partial w_j \big/ \partial x_i$. For all $\boldsymbol{\varphi} \in C_{\mathbf{0}}^\infty(X; \mathbb{R}^2)$, we have the following computations

$$\begin{aligned}
&\int_X \tilde{\mathbf{e}}(\mathbf{w}) : \tilde{\mathbf{e}}(\boldsymbol{\varphi}) \, dx \\
&= \frac{1}{2} \int_X \left[(\partial_2 w_2 - \partial_1 w_1)(\partial_2 \varphi_2 - \partial_1 \varphi_1) + (\partial_1 w_2 + \partial_2 w_1)(\partial_1 \varphi_2 + \partial_2 \varphi_1) \right] dx \\
&= \frac{1}{2} \Big[\ {}_{\mathscr{D}} \langle \partial_1 \varphi_1, (-\partial_2 w_2 + \partial_1 w_1) \rangle_{\mathscr{D}'} + \ {}_{\mathscr{D}} \langle \partial_2 \varphi_2, (\partial_2 w_2 - \partial_1 w_1) \rangle_{\mathscr{D}'} \\
&\qquad + \ {}_{\mathscr{D}} \langle \partial_2 \varphi_1, (\partial_1 w_2 + \partial_2 w_1) \rangle_{\mathscr{D}'} + \ {}_{\mathscr{D}} \langle \partial_1 \varphi_2, (\partial_1 w_2 + \partial_2 w_1) \rangle_{\mathscr{D}'} \Big] \\
&= \frac{1}{2} \Big[\ {}_{\mathscr{D}} \langle \varphi_1, (\partial_1 \partial_2 w_2 - \partial_1 \partial_1 w_1) \rangle_{\mathscr{D}'} + \ {}_{\mathscr{D}} \langle \varphi_2, (-\partial_2 \partial_2 w_2 + \partial_1 \partial_2 w_1) \rangle_{\mathscr{D}'}
\end{aligned}$$

$$
\begin{aligned}
&\quad + \ {}_{\mathscr{D}}\langle \varphi_1, (-\partial_1\partial_2 w_2 - \partial_2\partial_2 w_1)\rangle_{\mathscr{D}'} + \ {}_{\mathscr{D}}\langle \varphi_2, (-\partial_1\partial_1 w_2 - \partial_1\partial_2 w_1)\rangle_{\mathscr{D}'}\Big] \\
&= \frac{1}{2}\sum_{i=1}^{2} \ {}_{\mathscr{D}}\langle \varphi_i, -\Delta w_i\rangle_{\mathscr{D}'} = \frac{1}{2}\ {}_{\mathscr{D}}\langle \boldsymbol{\varphi}, -\Delta \mathbf{w}\rangle_{\mathscr{D}'} \\
&= \frac{1}{2}\int_X \nabla \mathbf{w} : \nabla \boldsymbol{\varphi}\, dx.
\end{aligned}
$$

Since $C_0^\infty(X;\mathbb{R}^2)$ is dense in $H_0^1(X;\mathbb{R}^2)$, we conclude that

$$
\int_X \tilde{\mathbf{e}}(\mathbf{w}) : \tilde{\mathbf{e}}(\boldsymbol{\varphi})\, dx = \frac{1}{2}\int_X \nabla \mathbf{w} : \nabla \boldsymbol{\varphi}\, dx, \quad \text{for all } \boldsymbol{\varphi} \in H_0^1(X;\mathbb{R}^2). \quad \square
$$

Therefore, in two dimensions, it is better in terms of mesh quality to extend the velocity field by $\mathbf{w}$ satisfying the following Laplace equation:

$$
-\Delta \mathbf{w} = \mathbf{0} \quad \text{in } X, \qquad \mathbf{w} = \mathbf{g} \quad \text{on } \partial X.
$$

On the other hand, if it is in three dimensions, the formula is a bit complicated because the terms do not cancel each other out as in the case of two dimensions, but it can be obtained as follows.

Proposition 4.0.2. *Let X be a bounded domain in $\mathbb{R}^3$. We suppose $\mathbf{w} \in H^1(X;\mathbb{R}^3)$. Then, the equation $-\Delta \mathbf{w} - \frac{1}{3}\nabla(\operatorname{div} \mathbf{w}) = 0$ in $\mathscr{D}'(X)$, is equivalent to the variational equation*

$$
\int_X \tilde{\mathbf{e}}(\mathbf{w}) : \tilde{\mathbf{e}}(\boldsymbol{\varphi})\, dx = 0, \ \textit{for all } \boldsymbol{\varphi} \in H_{\mathbf{0}}^1(X;\mathbb{R}^3).
$$

Proof. For any $\boldsymbol{\varphi} \in C_{\mathbf{0}}^\infty(X;\mathbb{R}^3)$, we have the following computations

$$
\begin{aligned}
&\int_X \tilde{\mathbf{e}}(\mathbf{w}) : \tilde{\mathbf{e}}(\boldsymbol{\varphi})\, dx \\
&= \int_X \left\{ \sum_{i=1}^{3} \Big(\partial_i w_i - \frac{1}{3}\operatorname{div}\mathbf{w}\Big)\Big(\partial_i \varphi_i - \frac{1}{3}\operatorname{div}\boldsymbol{\varphi}\Big) + \frac{1}{4}\sum_{i\neq j}(\partial_i w_j + \partial_j w_i)(\partial_i \varphi_j + \partial_j \varphi_i) \right\} dx \\
&= \int_X \left\{ \sum_{i=1}^{3} \partial_i \varphi_i \Big(\partial_i w_i - \frac{1}{3}\operatorname{div}\mathbf{w}\Big) - \frac{1}{3}\operatorname{div}\boldsymbol{\varphi}\left[\sum_{i=1}^{3}\Big(\partial_i w_i - \frac{1}{3}\operatorname{div}\mathbf{w}\Big)\right] \right. \\
&\qquad + \frac{1}{2}\Big[\partial_2\varphi_1(\partial_1 w_2 + \partial_2 w_1) + \partial_1\varphi_2(\partial_1 w_2 + \partial_2 w_1) \\
&\qquad\quad + \partial_2\varphi_3(\partial_2 w_3 + \partial_3 w_2) + \partial_3\varphi_2(\partial_2 w_3 + \partial_3 w_2) \\
&\qquad\quad \left. + \partial_3\varphi_1(\partial_3 w_1 + \partial_1 w_3) + \partial_1\varphi_3(\partial_3 w_1 + \partial_1 w_3)\Big] \right\} dx \\
&= \sum_{i=1}^{3} {}_{\mathscr{D}}\Big\langle \varphi_i, (-\partial_i\partial_i w_i + \frac{1}{3}\partial_i(\operatorname{div}\mathbf{w}))\Big\rangle_{\mathscr{D}'} \\
&\quad + \frac{1}{2}\Big\{ \ {}_{\mathscr{D}}\langle \varphi_1, (-\partial_1\partial_2 w_2 - \partial_2\partial_2 w_1)\rangle_{\mathscr{D}'} + \ {}_{\mathscr{D}}\langle \varphi_2, (-\partial_1\partial_1 w_2 - \partial_1\partial_2 w_1)\rangle_{\mathscr{D}'} \\
&\qquad + \ {}_{\mathscr{D}}\langle \varphi_3, (-\partial_2\partial_2 w_3 - \partial_2\partial_3 w_2)\rangle_{\mathscr{D}'} + \ {}_{\mathscr{D}}\langle \varphi_2, (-\partial_2\partial_3 w_3 - \partial_3\partial_3 w_2)\rangle_{\mathscr{D}'} \\
&\qquad + \ {}_{\mathscr{D}}\langle \varphi_1, (-\partial_3\partial_3 w_1 - \partial_1\partial_3 w_3)\rangle_{\mathscr{D}'} + \ {}_{\mathscr{D}}\langle \varphi_3, (-\partial_1\partial_3 w_1 - \partial_1\partial_1 w_3)\rangle_{\mathscr{D}'} \Big\} \\
&= \sum_{i=1}^{3} {}_{\mathscr{D}}\Big\langle \varphi_i, \Big(-\frac{1}{2}\Delta w_i - \frac{1}{6}\partial_i(\operatorname{div}\mathbf{w})\Big)\Big\rangle_{\mathscr{D}'} \\
&= {}_{\mathscr{D}}\Big\langle \boldsymbol{\varphi}, \Big(-\frac{1}{2}\Delta \mathbf{w} - \frac{1}{6}\nabla(\operatorname{div}\mathbf{w})\Big)\Big\rangle_{\mathscr{D}'} \\
&= \frac{1}{2}\int_X \nabla \mathbf{w} : \nabla \boldsymbol{\varphi} + \frac{1}{3}(\operatorname{div}\mathbf{w})(\operatorname{div}\boldsymbol{\varphi})\, dx = 0.
\end{aligned}
$$

In view of the last line above, varying φ, we get the desired result. $\square$

From the previous proposition, we infer that, in three dimensions, it is better in terms of mesh quality to extend the velocity field by $\mathbf{w}$ satisfying the following problem:

$$
-\Delta \mathbf{w} - \frac{1}{3}\nabla(\operatorname{div}\mathbf{w}) = \mathbf{0} \quad \text{in } X, \qquad \mathbf{w} = \mathbf{g} \quad \text{on } \partial X.
$$

5. Conclusion

We have presented in this investigation some further developments and applications of the so-called 'comoving mesh method' or CMM for solving mean-curvature flow problems. Moreover, we have demonstrated how CMM can be applied to solve the one-phase Stefan problem. Additionally, with the smooth extension obtained using the linear elasticity equation instead of the Laplace equation, we have provided two properties of CMM relating to mesh quality. It was found that using the Laplace equation for smoothly extending the normal flows is optimal in the case of two dimensions. However, in the case of three dimensions, an additional expression in terms of the divergence of the smooth extension appears in the main equation.

In our next investigation, we will apply the method to more general moving boundary problems, such as the one-phase quasi-stationary Stefan problem with Gibbs–Thomson law and kinetic undercooling, while considering three-dimensional cases.

Acknowledgments

The authors would like to express their gratitude to the reviewer for his/her comments in the earlier version of the paper. The work of JFTR is partially supported by JST CREST Grant Number JPMJCR2014 and JSPS KAKENHI Grant Number JP23K13012. The work of MK is supported by JSPS KAKENHI Grant Numbers JP20KK0058 and JP20H01812.

References

[1] H. Azegami, A solution to domain optimization problems, Trans. Jpn. Soc. Mech. Eng. Ser. A 60 (1994) 1479–1486, in Japanese.
[2] H. Azegami, Shape Optimization Problems, Springer Optimization and Its Applications, Springer, Singapore, 2020.
[3] D.L. Chopp, Computation of self-similar solutions for mean curvature flow, Exp. Math. 3 (1) (1994) 1–15.
[4] J. Crank, Free and Moving Boundary Problems, Clarendon Press, 1984.
[5] Q. Dai, Y. Lei, B. Zhang, D. Feng, X. Wang, X. Yin, A practical adaptive moving-mesh algorithm for solving unconfined seepage problem with galerkin finite element method, Sci. Rep. 9 (Art. 6988) (2019) 15.
[6] G. Duvaut, J.L. Lions, Inequalities in Mechanics and Physics, Springer Berlin, Heidelberg, 1976.
[7] G. Dziuk, An algorithm for evolutionary surfaces, Numer. Math. 58 (1991) 603–611.
[8] K. Eppler, H. Harbrecht, Efficient treatment of stationary free boundary problems, Appl. Numer. Math. 56 (2006) 1326–1339.
[9] A. Ern, J.-L. Guermond, Theory and practice of finite elements, in: Applied Mathematical Sciences, Springer-Verlag, New York, NY, 2004.
[10] J. Escher, G. Simonnet, Classical solutions of multidimensional Hele-Shaw models, SIAM J. Math. Anal. 28 (5) (1997) 1028–1047.
[11] M. Flucher, M. Rumpf, Bernoulli's free-boundary problem, qualitative theory and numerical approximation, J. Reine. Angew. Math. 486 (1997) 165–204.
[12] A. Friedman, Free-boundary problem in fluid dynamics, Astérisque, Soc. Math. France 118 (1984) 55–67.
[13] M. Gage, R. Hamilton, The heat equation shrinking convex plane curves, J. Differential Geom. 23 (1986) 69–96.
[14] M. Grayson, The heat equation shrinks embedded plane curves to round points, J. Differential Geom. 26 (1987) 285–314.
[15] B. Gustafsson, A. Vasilév, Conformal and potential analysis in Hele-Shaw cell, in: Advances in Mathematical Fluid Mechanics, Bikhäuser, Basel, 2006.
[16] G. Huisken, Flow by mean curvature of convex surfaces into sphere, J. Differential Geom. 20 (1984) 237–266.
[17] M. Kimura, Numerical analysis for moving boundary problems using the boundary tracking method, Jpn. J. Ind. Appl. Math. 14 (1997) 373–398.
[18] M. Kimura, Geometry of Hypersurfaces and Moving Hyper Surfaces in R^m for the Study of Moving Boundary Problems, in: Jindřich Nečas Center for Mathematical Modeling Lecture notes, vol. IV, Matfyz Press, 2008, pp. 39–93, Ch. 2.
[19] M. Kimura, H. Notsu, A level set method using the signed distance function, Jpn. J. Ind. Appl. Math. 19 (2002) 415–446.
[20] A.A. Lacey, M. Shillor, Electrochemical and electro-discharge machining with a threshold current, IMA J. Numer. Anal. 39 (2) (1987) 121–142.
[21] V.D. Liseikin, Grid Generation Methods, third ed., Springer, Cham, 2017.
[22] A.M. Meirmanov, The Stefan Problem, De Gruyter, 2011.
[23] H. Murakawa, An efficient linear scheme to approximate nonlinear diffusion problems, Jpn. J. Ind. Appl. Math. 35 (1) (2018) 71–101.
[24] K. Sakakibara, Y. Shimoji, S. Yazaki, A simple numerical method for Hele-Shaw type problems by the method of fundamental solutions, Jpn. J. Ind. Appl. Math. 39 (2022) 869–887.
[25] K. Sakakibara, S. Yazaki, A charge simulation method for the computation of Hele-Shaw problems, RIMS Kôkyûroku 1957 (2015) 116–133.
[26] K. Sakakibara, S. Yazaki, Structure-preserving numerical scheme for the one-phase Hele-Shaw problems by the method of fundamental solutions, Comput. Math. Methods 1 (2019) e1063.
[27] Y. Sunayama, M. Kimura, J.F.T. Rabago, Comoving mesh method for certain classes of moving boundary problems, Jpn. J. Ind. Appl. Math. 39 (2022) 973–1001.
[28] M. Tabata, Galerkin-characteristics finite element method: theory and applications (the latest developments in theory and application on scientific computation), RIMS Kôkyûroku 1791 (4) (2012).
[29] A. Vasintin, Introduction to Stefan-Type Problems, in: Handbook of Differential Equations: Evolutionary Equations, vol. 4, Elsevier, New York, NY, 2008, pp. 377–484, Ch. 8.